Accepted Manuscript

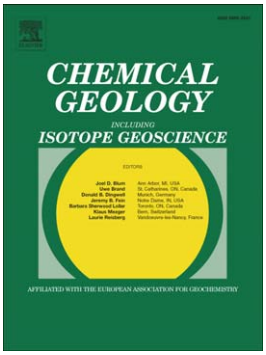

Intrinsic solidification behaviour of basaltic to rhyolitic melts: A cooling rate experimental study

Francesco Vetere, Gianluca Iezzi, Harald Behrens, Andrea Cavallo, Valeria Misiti, Marcel Dietrich, Jaayke Knipping, Guido Ventura, Silvio Mollo

PII: S0009-2541(13)00264-7
DOI: doi: 10.1016/j.chemgeo.2013.06.007
Reference: CHEMGE 16917

To appear in: *Chemical Geology*

Received date: 10 April 2013
Revised date: 7 June 2013
Accepted date: 8 June 2013

Please cite this article as: Vetere, Francesco, Iezzi, Gianluca, Behrens, Harald, Cavallo, Andrea, Misiti, Valeria, Dietrich, Marcel, Knipping, Jaayke, Ventura, Guido, Mollo, Silvio, Intrinsic solidification behaviour of basaltic to rhyolitic melts: A cooling rate experimental study, *Chemical Geology* (2013), doi: 10.1016/j.chemgeo.2013.06.007

Intrinsic solidification behaviour of basaltic to rhyolitic melts: a cooling rate experimental study

Francesco Vetere[1,3], Gianluca Iezzi[1,2], Harald Behrens[3], Andrea Cavallo[2], Valeria Misiti[2], Marcel Dietrich[3], Jaayke Knipping[3], Guido Ventura[2], Silvio Mollo[2]

[1]Dipartimento di Ingegneria e Geologia, Università G. d'Annunzio, via dei Vestini 31, 66100 Chieti Italy.

[2]Istituto Nazionale di Geofisica e Vulcanologia, Roma, via di Vigna Murata 605 00167 Roma, Italy.

[3]Institute for Mineralogy, Leibniz University of Hannover, Callinstr. 3, Hannover, D-30167, Germany

To be submitted to:

Chemical Geology

Author for correspondence:

Gianluca Iezzi, email: g.iezzi@unich.it, phone: +39 0871 3556147, fax: +39 0871 3556048

ABSTRACT

Dynamic cooling-induced solidification experiments were run using six silicate glasses along the basalt - rhyolite join (B_{100}= 100 wt % of basalt, R_{100}= 100 wt % of rhyolite), i.e. B_{100}, $B_{80}R_{20}$, $B_{60}R_{40}$, $B_{40}R_{60}$, $B_{20}R_{80}$ and R_{100}; the glasses directly quenched from 1300 °C after a dwell of 120 minutes (experiment E0) contain 50-400 ppm H_2O, << 1 area% µm-sized bubble, and Fe^{2+}/Fe_{tot} between 0.34 and 0.46. Experiments were performed in Pt capsules at room pressure and fO_2 of air, between 1300 and 800 °C using three different cooling rates of 0.0167, 3 and 30 °C/min; these cooling rates were run two times: E1-E2 experiments at 0.0167°C/min, S1-E3 at 3 °C/min, and E4-E5 at 30 °C/min. In experiments E1 to E5, samples were annealed for 120 minutes at 1300 °C, whereas in the experiment S1 the samples were firstly heated for 30 minutes at 1400 °C followed by a dwell time of 2400 minutes at 1300°C before cooling. In the experiments a preferential crystallization was not observed at the melt/gas interface. B_{100}, $B_{80}R_{20}$ and $B_{60}R_{40}$ run-products have a low tendency to preferentially crystallize on Pt walls, while $B_{40}R_{60}$, $B_{20}R_{80}$ and R_{100} are not affected by the presence of Pt substrata. All run-products show very homogeneous textures, except for $B_{60}R_{40}$ and $B_{40}R_{60}$ at 0.0167°C/min in the E1 experiment. The duplicates of $B_{40}R_{60}$ and $B_{60}R_{40}$ at 0.0167°C/min and B_{100} at 30 °C/min show relatively large differences in crystal content (> 4 and < 14 area%). $B_{40}R_{60}$ and $B_{60}R_{40}$ duplicated run-products have the same amount of early-crystallized clinopyroxene and spinel, but different contents in lately-formed plagioclase. The run-products with the same starting composition from E3-S1 (3 °C/min) show a high reproducibility in terms of crystal shape, size, and amount (< 4 area%). This demonstrates that the crystallization path is not affected by the different heat treatment above the liquidus temperature, i.e. the time scale of structural re-equilibration (relaxation) and chemical re-homogenization are shorter than our experimental time scale. Possible chemical

heterogeneities on a length scale of several micrometers for R_{100} and several hundreds of micrometers for B_{100} can be removed at 1300 °C within 120 minutes. A heat treatment at 1300 °C for 120 minutes significantly reduces the amount of µm-sized bubbles, potentially responsible for the onset of nucleation and unreveals the intrinsic solidification of silicate melts. The experimental reproducibility is low when the cooling path intersects the tip of the time-temperature-transformation (TTT) curves, i.e. when the nucleation rate is near its maximum (I_{max}). In that case, even small thermal variations in cooling rate and local composition can have large effects on phase abundance and crystal size. Dynamic crystallization experiments can be properly interpreted and compared only if they are texturally homogeneous and the physico-chemical state of the superheated silicate liquid is known. The solidification conditions used in this study mirror those of aphyric lavas and dikes emplaced at shallower crustal levels.

Keywords: cooling kinetics, nucleation, solidification, superheating, reproducibility, silicate melt.

1. INTRODUCTION

The time-temperature history experienced above the liquidus may have strong influence on the crystallization path of a silicate melt and, hence, on texture and composition of crystallised phases. A silicate liquid kept for long times and/or at high temperatures above its liquidus will show the lowest nucleation rate during successive cooling and will show the highest incubation time of the first crystallising phase in the sub-liquidus region (Kirkpatrick, 1981; Tsuchyama, 1983; Lasaga, 1997; Pupier et al., 2008; Hammer, 2008). This effect has been explained by an incomplete re-equilibration of short-range order and/or polymeric configurations acquired at liquidus or superliquidus conditions that metastably persist during cooling below liquidus temperatures (Kirkpatrick, 1981; Corrigan, 1982; Tsuchyama, 1983; Hammer, 2008). On the other hand, microscopic gas bubbles, chemical heterogeneities or "solid foreign particles" that are not fully eliminated during heat treatments and persist in a silicate melt at sub-liquidus temperatures may promote crystallization (Dowty, 1980; Lofgren, 1980 and 1983; Davies and Ihinger, 1998; Armienti, 2008; Pupier et al., 2008; Iezzi et al., 2008 and 2011). A superheating above the liquidus is required to remove such memory effects and to unravel the intrinsic solidification behaviour of natural silicate melts as a function of composition. However, direct and systematic experimental investigations are not available and physico-chemical features (bubbles, volatile content, un-melted crystals, etc.) of a silicate melt before its solidification are generally uncharacterised; this may limit the interpretation of kinetics data in a single run-product as well as the comparison of experimental results, even derived by the same initial melt.

Reproducibility and homogeneity of cooling-induced solidified products has been poorly investigated and crystallization kinetics is not sufficiently explored for natural melt systems. The few experimental studies reported in the literature mainly focus on basalts, and,

subordinately, on andesites, latites, trachytes and rhyolites (Donaldson et al., 1975; Kirckpatrick, 1981; Lofgren, 1980 and 1983; Berkebile and Dowty, 1982; Tsuchiyama, 1983; Couch, 2003; Hammer, 2006; Pupier et al., 2008; Iezzi et al., 2011 and references therein). Runs on SiO_2-poor melts at atmospheric pressure and fO_2 lower than air show that the sample holder (wire or capsule) and the container material (Pt or Au) can significantly influence the results of solidification experiments (Dowty, 1980; Lofgren, 1980; Berkebile and Dowty, 1982; Tsuchyama, 1983; Pupier et al., 2008). On the other hand, intermediate (andesitic and latitic) to evolved (trachytic and rhyolitic) silicate melts appear to be poorly or not affected by the sample container (Couch, 2003; Iezzi et al., 2008 and 2011; Mollo et al., 2012a). This difference probably relies on the rapid diffusion in silica-poor melts allowing fast transport to existing nuclei. Additionally, surface tension between the nucleus, the melt and (possibly) foreign substrates plays a crucial role in nucleation kinetics (Dowty, 1980; Fokin et al., 2003; Iezzi et al., 2008 and 2011). However, the controlling parameter for nucleation and growth were poorly constrained for these relatively SiO_2-rich melt systems.

In order to constrain the variation of intrinsic crystallization behaviours of natural silicate melts as a function of their composition, the role of superheating before cooling and the degree of textural reproducibility, we performed crystallization experiments on six silicate melt compositions ranging from basalt to rhyolite: B_{100}, $B_{80}R_{20}$, $B_{60}R_{40}$, $B_{40}R_{60}$, $B_{20}R_{80}$ and R_{100}, where B_{100}= basalt and R_{100}= rhyolite (numbers are wt.% in each mixture). These compositions cover the most part of volcanic rocks. The effect of cooling rate was explored using rates of 0,0167, 3 and 30 °C/min between 1300 and 800 °C. The results of this study show that the superheating effect can be eliminated by annealing all these melts at 1300 °C for 120 minutes before cooling (Fig. 1), the majority of cooling-induced crystallization can be well reproduced, and the intrinsic solidification behaviour from basalt to rhyolite are strongly

different, being basalt crystal-rich (> 50 area%) at 30 °C/min and rhyolite glassy even at 0.0167 °C/min.

2. STARTING MATERIALS, EXPERIMANTAL AND ANALYTICAL TECNIQUES

2.1 Starting materials

Six different silicate compositions were prepared along the sub-alkaline join basalt-rhyolite. We used natural samples from Iceland (B_{100} = basalt) and Lipari Island (Aeolian Islands, Italy, R_{100} = rhyolite) to prepare glasses of the end-members (Table 1). About 100 g of these two rocks were crushed and then melted in a Pt crucible at 1600 °C in air for 4 hours. For quenching, the basalt was poured on a metal plate. Due to its high viscosity the rhyolite could be quenched only inside the crucible by putting it into a water bath. The two recovered glasses were crushed again and re-melted twice at the same conditions, with an intermediate grinding step, to obtain chemically homogeneous glass materials. About 70 g of each glass was crushed and sieved to obtain 1:1 mixtures by weight of two different grain sizes ranges (<200 and 200–500 μm); such mixture minimize the number of small bubbles after subsequent re-melting. The two powders were then mixed to produce the four intermediate compositions ($B_{80}R_{20}$, $B_{60}R_{40}$, $B_{40}R_{60}$, $B_{20}R_{80}$). Each of these batches was then melted at 1600 °C for 4 hours in air and rapidly quenched ($B_{80}R_{20}$ and $B_{60}R_{40}$ were poured on a metal plate, $B_{40}R_{60}$ and $B_{20}R_{80}$ were cooled within the crucible in the water bath). The procedure was repeated twice with intermediate grinding to improve homogeneity. Thus, six homogeneous glass starting materials with systematic chemical variations were obtained. Several glass fragments of each starting composition were analyzed by EPMA (see below); the average

compositions of the glasses are reported in Table 1 and classified according to TAS (Le Maitre et al., 2002). Several other glass fragments were used to quantify the H_2O amount by FTIR spectroscopy, and the iron speciation by a modified Wilson method (see below).

2.2 Experimental strategy and techniques.

The effect of cooling rate was systematically investigated using rates of 0.0167 (E1-E2), 3 (E3) and 30 (E4-E5) °C/min between 1300 and 800 °C. Afterwards the samples were rapidly quenched. In experiments E1, E2 and E3 all six compositions were used while the highest cooling rate (in E4 and E5) was only applied to B_{100} (Table 2). For all experiments labelled with E, the heating rate was 7 °C/min up to 1300 °C and then followed by a dwell time of 120 minutes at 1300 °C. To characterize ex-situ the physico-chemical state of all the six melts at the end of this pre-heating, in an additional experiment the samples were directly quenched from 1300 °C to room temperature in water (experiment E0). In order to investigate the role of pre-heating, an initial heating for 30 minutes at 1400 °C was followed by a long dwell of 40 hours at 1300 °C was applied to the above mentioned starting materials using a cooling rate of 3 °C/min (experiment S1). The reproducibility of the experiments was checked by duplicates at cooling rates of 0.0167and 30 °C/min (E1-E2 and E4-E5).

To perform the 32 experiments, mm-sized glass fragments were loaded into Pt tubes (4 mm in diameter and 15-20 mm in length). Each capsule contains ~50 mg of glass chips. All the experiments were run at atmospheric pressure and air redox state.

The experiments E1, E2, E3 and S1 were performed at the Dipartimento di Ingegneria e Geologia (University G. d'Annunzio, Chieti, Italy), in a vertical rapid-quench Protherm PTF16/50/450 furnace equipped with a EUROTHERM controller. The temperature was monitored by two R-type (Pt87Rh13-Pt) thermocouples with an accuracy of ± 3 °C at the

inner side of the ceramic tube and in direct contact with the sample assembly, which consists of up to six capsules held together with Pt wires. As determined by exchanging the position of the internal thermocouple, the temperature variation within the assembly is less than 5 °C.

The E4-E5 experiments were run at the Institute of Mineralogy in Hannover (Leibniz University, Hannover, Germany), using the Pt sample holder of an apparatus normally used for Karl-Fischer titration (Behrens et al., 1996). Heating was achieved with a high frequency generator Linn$^{(R)}$-HTG 1000/1.3 and controlled by a EUROTHERM(R) type 818 controller/programmer. The temperature was measured with a Pt/Pt90Rh10 (S-type) thermocouple about 5 mm below the center of the samples which were inserted within Pt capsules in the Pt sample holder. Closed capsules were used in these experiments to separate the melt from the argon atmosphere in the apparatus, i.e. to avoid reduction of the melt. After closing the chamber, the heating/cooling program was launched. Quenching has been achieved by switching off the high frequency generator and rapidly taking out the sample holder and rolling it on a metal plate. Due to the high heat conductivity of Pt capsules in Pt sample holder the temperature drops down to room temperature within less than 5 seconds.

E0 experiments were also run in Hannover, but using a tube furnace GERO HTRV model 100-250. Temperature was monitored by two S-type thermocouples with an accuracy of ± 3 °C. The first thermocouple was in contact with the sample assembly and the second one was placed at the inner side of the ceramic tube. All the capsules in each experiment were located at < 1 cm from the central thermocouple. Temperature variations were less than 5 °C within the sample assembly.

2.3 Analytical techniques.

All the recovered run-products have been mounted in epoxy, ground flat and polished, such to expose the centre of the melt body as well as the contacts to air and to the capsule walls. The phases with at least an available diameter comprised between 1 and 3 μm were characterized with a Jeol FE-SEM 6500F equipped with an energy dispersive x-ray (EDX) microanalysis system at the HP-HT laboratory of INGV. Representative BSE images on each section were recorded with the SEM at magnifications of 150X, 400X, 800X, 1500X and 3000X. Area% of the different phases was determined for all images showing well resolved crystals. Typically, the considered BSE images represent areas of ~10^3 μm^2 up to ~10^6 μm^2. At least four BSE images recorded in different parts of the section were evaluated to check for homogeneity. In some cases a larger number of 8 to 36 images were studied to improve statistics (see Table 2). Image analysis was performed by the Image-ProPlus 6.0 software, to count area% of each phase as a function of their grey levels. Based on differences in grey levels, area% of glass, clinopyroxene, spinel, plagioclase phases were quantified. We did not apply a stereological correction, in order to avoid any mathematical manipulation of data. At the end, about 300 BSE images were considered.

2.4 Water content and iron speciation.

To measure the water contents of the starting glasses, absorption spectra were recorded in the mid-infrared (MIR) using a Bruker IFS88 FTIR spectrometer coupled with an IR-ScopeII microscope (operation conditions: MCT narrow range detector; globar light source and KBr beamsplitter for MIR). Spectral resolution was 2 cm^{-1} in the MIR and 50-100 scans were accumulated for each spectrum. The spot size applied in analyses was

approximately 100×100 µm. The analysed area was checked optically before FTIR measurements to avoid any bubbles, cracks or impurities. The evaluation of the IR spectra requires the knowledge of the density and the thickness of the glass section. Doubly polished glass plates of 50-300 µm thickness were prepared from the experimental products. The thickness of each section was measured with a digital micrometer (Mitutoyo; precision ± 2 µm). The density of the glasses was calculated after Klöß (2000) and results are reported in Table 1.

For determination of ferrous-ferric ratios, the modified colorimetric method by Wilson (1960) was used (Schuessler et al., 2008). From 6 to 9 mg of chips of the starting glasses were dissolved with concentrated HF to which a solution of ammonium vanadate in 5 M sulphuric acid was added. The released ferrous iron reacts with V^{5+} forming V^{4+} and ferric iron (reaction $Fe^{2+} + V^{5+} = Fe^{3+} + V^{4+}$). The initial redox state of the glass is preserved in the solution as the reaction products are more stable with respect to oxidation in air than ferrous iron. We added saturated hot boric acid (353 K) instead of beryllium sulphate as proposed by Wilson (1960) to neutralize excess HF and to bring eventually formed fluorides back into solution after complete sample dissolution at room temperature. Using an ammonium acetate buffer, the Fe^{2+} is regenerated by adjusting a pH value of ~5. For the colorimetric analysis 2:2'bipyridyl was added which forms a stable complex with Fe^{2+}. To quantify the concentration of this complex we have used the characteristic absorption band at 523 nm. Measurements of concentrations of ferrous Fe and total Fe were made on the same solution using UV/VIS spectrometer Zeiss Specord S10. Results are reported again in Table 1.

3. RESULTS

Four major phases are present in the run products: glass, clinopyroxene, spinel and plagioclase (Table 2); in few run-products, minor amounts (<< 1 area%) of olivine, orthopyroxene and melilite were also found. Run-products contain few mm-sized bubbles, probably due to trapped air. On the other hand the total amount of µm-sized bubbles dispersed in matrix glasses are always << 1 area%.

The textural features of each run-product in comparison to the duplicates are shown in Figures 2a (E1-E2 experiments at 0.0167°C/min), 2b (S1-E3 experiments at 3 °C/min), and 2c (E4-E5 experiments at 30 °C/min). In R_{100} melts, crystals were observed only at cooling rates of 0.0167and 3 °C/min, with amounts ≈ 1 area% and so these samples are not displayed in Fig. 2. Crystal size and content progressively increases from R_{100} to B_{100} compositions for a fixed cooling rate. In each bulk composition, a decrease in crystal content and average crystal size, and a preference of dendritic shapes (Figures 2a, 2b and 2c) occur as cooling rate increases.

The homogeneity of each run product was evaluated using the BSE images recorded in different regions of the samples. Criteria for homogeneity are the fraction of phases quantified by image analyses, as well as crystal size and shape evaluated qualitatively on BSE images (Figures 2a, 2b and 2c). As a rough threshold we consider samples with standard deviations of area% of phases < 4 as homogeneous (H) and those with higher variations as inhomogeneous (IN). Using that criterion, the majority of run-products show a homogeneous texture at the millimetre scale. Samples which are classified as inhomogeneous vary mainly in plagioclase size and content. In sample $B_{40}R_{60}$ from E1, some regions are free of plagioclase while others have large fractions, resulting in a large variation of 20.0 ± 12.6 area% (Table 2). As a consequence, the amount of glass largely change, i.e. 67.1 ± 10.9

area%. Sample $B_{60}R_{40}$ from E1 also shows significant variation in plagioclase (40.4 ± 7.2 area%) associated with variations in clinopyroxene and glass content (Table 2). The homogeneity criterion describes the bulk of samples.

A slight enrichment in spinel content at the interface with the Pt capsule compared to the bulk was sometimes but not always observed from B_{100} to $B_{60}R_{40}$ compositions. It is not clear whether the relatively higher abundance of spinel, that is a typical early-formed phase, is due to chemical heterogeneities near the capsule wall or to preferred nucleation at the melt/Pt interface (see below). In Table 2 experiments are discriminated with respect to spinel enrichment at the melt/Pt interface by A (absent) or P (present). It is worth noting that only the rim of few micrometers of run-products near the noble metal is affected by such behaviour. Furthermore, an enrichment of phases was never observed around μm-sized bubbles or at the melt/air interface. These interfaces do not act as preferential nucleation sites in our experiments, in perfect agreement with the conclusion carried out by Mollo et al. (2012a). On the other hand, early-formed spinel was sometimes observed to be surrounded by clinopyroxene, i.e. in $B_{40}R_{60}$ melts from S1 and E3 (cooling rate of 3 °C/min), indicating that heterogeneous nucleation of clinopyroxene plays a role in these experiments (Fig. 2b).

The textural reproducibility of experiments run under the same cooling rate, i.e. E1-E2, S1-E3 and E4-E5, was evaluated by comparing area% of crystals, as well as the crystal size and shape (Table 2 and Figures 2, 3, 4). A good reproducibility was found in the majority of run-products solidified under the same cooling rate, with differences in crystal content < 4 area% (Table 2). However, the duplicated run-products $B_{60}R_{40}$ and $B_{40}R_{60}$ in the E1-E2 have differences in crystal content of 6.1 and 13.6 area%, respectively, whereas the difference is 9.4 area% between the two run-products in E4-E5 (Table 2). The two $B_{40}R_{60}$ samples largely differ in plagioclase content (E1: 20.0 ± 12.6 area%; E2: 2.3 ± 1.2 area%). Considering the inhomogeneity of the sample from E1, this observation points to a difficulty in plagioclase

nucleation, frequently observed in rapidly cooled basaltic melts (Del Gaudio et al., 2010; Mollo et al., 2011). Crystallization problems of plagioclase are probably also the reason for the poor reproducibility of the B_{100} samples from E4-E5. Plagioclase is expected to as a stable phase during cooling but was not formed at the high cooling rate of 30 °C/min (as well as at a cooling rate 3 °C/min).

4. DISCUSSION

The run-products from S1-E3 give clear evidence that heat treatment for 2 hours at 1300°C is sufficient to remove any memory effect in rhyoltic to basaltic melts for the given experimental conditions. However, a crucial question remains: what super heating conditions are required to destroy specific sites for heterogeneous nucleation within the melt? One possible issue is an incomplete structural (SRO: short range order) rearrangement inherited by a silicate melt above its liquidus. The time scale τ of structural re-equilibration (relaxation) of silicate melts can be estimated by the Maxwell relation

$$\tau = \frac{\eta}{G} \qquad (1)$$

where η is the viscosity of the melt and G is the shear modulus; G varies by less than a factor of ten with a mean value of 10 GPa (Dingwell and Webb, 1990; Moynihan, 1995; Dingwell, 1995; Richet, 2002; Webb, 1997 and 2005). For a silicate melt, the measured macroscopic (viscosity) relaxation reflects the exchange of Si among silicate species in the melt. From a molecular perspective, relaxation of Si is the slowest of all cations in a silicate liquid. This implies that other chemical species re-equilibrate faster than Si-bearing ones (Stebbins, 1995; Webb, 1997 and 2005; Richet, 2002; Dingwell, 2006).

Using data from literature (Hess and Dingwell, 1996; Giordano and Dingwell, 2003; Zhang et al., 2003; Misiti et al., 2009), the structural relaxation time was estimated considering the water contents reported in Table 1 in the viscosity calculation. In Figure 5 and 6 data are plotted based on viscosity equations for rhyolite from Zhang et al. (2003) and for Etna basalt from Giordano and Dingwell (2003). Computation of viscosity after Hess and Dingwell (1996) for rhyolite and after Misiti et al. (2009) for Stromboli basalt agree within 0.2 log units with these calculations at the corresponding liquidus temperatures. Assuming G = 10 GPa, the time needed for complete relaxation at 1300 °C is 10^{-10} and 10^{-7} seconds for B_{100} and R_{100}, respectively. Even at their respective liquidus temperatures τ is low as 0.6 seconds for the rhyolite (1000 °C) and 10^{-5} seconds for the basalt (1200 °C). Relaxation times for the other four melt compositions are intermediate. These estimates demonstrate that the superheating effect cannot be ascribed to un-relaxed short range features "recorded" by a silicate melt above its liquidus; in other words, the melt structure at the liquidus temperature can be considered independent from the thermal-time path experienced at the superliquidus region, even for extremely fast variations of temperature.

Another important factor that must be considered for the possible role of heat treatment on successive crystallization behaviours is the presence of chemical inhomogeneities, distinct phases in the melt, and differences between liquidus temperatures and superheating treatment of the starting materials from 370 °C (B_{100}) to 560 °C (R_{100}). Inhomogeneities can originate from compositional variations already present within the starting glasses as well as from surface contaminations of the glass fragments used in the experiments. Ghost boundaries observed frequently in crystallization experiments, i.e. nucleation at the contacts of former glass grains, can be explained by such chemical inhomogeneities (Roskovz et al., 2005). If these inhomogeneities or distinct phases are soluble in the melt, the time and length scale of re-homogenisation can be estimated from diffusivities of network forming cations such as Al

and Si. Diffusion coefficients for such species are correlated to viscosity by the Eyring relationship (Chakraborty, 1995):

$$D_\eta = \frac{k \cdot T}{\lambda \cdot \eta} \qquad (2)$$

where D_η is the diffusivity, k is the Boltzmann constant, T is the absolute temperature, λ is the characteristic jumping distance (typically around 3 Å in silicate melts), and η is the viscosity. The diffusion length

$$x = \sqrt{2 D_\eta t} \qquad (3)$$

can be considered as the minimum homogenisation distance in a melt within a time t, for a given diffusivity and, hence, given temperature T. Using the viscosity data calculated for B_{100} and R_{100} end-member melt compositions (see before), we constructed a diagram relating the diffusion length of the least mobile cations, i.e. Si and Al, with time and temperature (Figure 6). A dwell time of 120 minutes at 1300 °C used for E3, as well as for E1, E2, E4 and E5 experiments, allow a re-homogenisation for B_{100} and R_{100} end-member melts over distances of about 350 and 1.5 µm, respectively (Figure 6). On the other hand, the heat treatment of 30 minutes at 1400 °C and subsequent of 40 hours at 1300°C in the experiment S1 will homogenize compositional variations in B_{100} and R_{100} liquids over about 1250 and 8 µm, respectively (Figure 6). The high reproducibility of run-products crystallised in S1-E3 experiments demonstrates that possible presence of chemical heterogeneities within rhyolitic melts are smaller than 2 µm. It is worth noting that we can expect marked differences in the run-products when using a fine-grained glass powder as starting material, i.e. a preferred nucleation at former contacts of glass grains.

The above considerations are restricted to heterogeneities which can be dissolved in the melt. Insoluble particles or bubbles may survive even to long term annealing and may act as

heterogeneous nucleation sites (Dowty, 1980; Lofgren, 1980 and 1983; Davies and Ihinger, 1998; Pupier et al., 2008; Iezzi et al., 2008 and 2011). The physico-chemical state of the six starting compositions at the end of the pre-heating were directly investigated after a dwell time of 2 hours at 1300 °C (E0) by rapidly quenching each sample in a water bath. Spectroscopic, chemical and image analyses show: a) Fe^{2+}/Fe_{tot} between 0.34 and 0.45, b) dissolved water amounts below 400 ppm (Table 1), c) absence of any solid (un-melted) particles and d) an amount of << 1 area% of µm-sized bubbles in the melt. Therefore, only µm-sized bubbles could eventually act as heterogeneous sites in these melts, according to former experimental results (Davis and Ihinger, 1998; Muller et al., 2000; Pupier et al., 2008; Sycheva, 2009; Schiavi et al., 2010). However, we did not observe in our experiments a direct and significant effect on crystal nucleation due to the presence of a low amount of µm-sized bubbles in the melt. On the other hand, assuming that the very low amount of µm-sized bubbles affect the initial nucleation of crystals, it is here possible to depict a general conclusion; the high reproducibility of the corresponding run-products in the S1-E3 experiments demonstrates that this amount of µm-sized bubbles after a long heat treatment (S1) and after 120 minutes at 1300 °C (E3) are the same.

Our experimental observations on run-products from S1-E3, heat treated before cooling as in our study (1300 °C per 120 minutes), agree with the pioneering conclusion by Gibb (1974): "*The extent to which this basaltic liquid can be supercooled without the crystallization of plagioclase is independent of the time it is held above the liquidus or the temperature in excess of the liquidus to which it is heated*". As concerns the possible effect of the temperature difference between the liquidus temperature and the experimental starting temperature, Tsuchyama (1983) shows that superheating effects on nucleation in the diopside-anorthite system is lacking at about 40 °C above the liquidus (regardless the time duration), or at any fixed superliquidus temperature and experimental duration longer than 45 minutes.

These experimental observations, reported by Tsuchyama (1983), suggest that the "superheating effect" was related to kinetics necessary to eliminate foreign sites, possibly to reduce as much as possible the amount of µm-sized bubbles. Results from Tsuchyama (1983) have been recently corroborated by those from Mollo et al. (2012b). The authors have investigated the cooling kinetics of a trachybasalt from Mt. Etna volcano (Sicily, Italy) whose liquidus temperature is 1211 °C, at atmospheric pressure. Two different pre-heating treatments were performed by using a superliquidus temperature of 1250 °C and 1400 °C (39 °C and 189 °C above the liquidus) for 30 and 180 minutes, respectively. Then the melt was cooled under two different rates. By comparing run products, the authors did not observed significant variations, for example, no delay of crystal nucleation and no change in phase assemblage and phase proportion. Consequently, foreign sites that can induce crystal nucleation did not survive to thermal pre-treatments. In this view, the present study extents results from Tsuchyama (1983) and Mollo et al. (2012b) to a large range of melt compositions, providing that "superheating effects" vanish over a time scale of at least to 2 hours.

A preferential crystallization of spinel near Pt substrata has been observed for all the run-products with composition between B_{100} and $B_{60}R_{40}$, whereas $B_{40}R_{60}$ and R_{100} compositions are unaffected by the sample container (Table 2). This is consistent with previous crystallization experiments indicating that SiO_2-poor melts are more susceptible than SiO_2-rich melts to nucleate on sample holders, especially at low fO_2 conditions (Davis and Ihinger, 1998; Pupier et al., 2008; Swanson, 1977; Fenn, 1977; Couch, 2003; Martel and Schmidt, 2003; Iezzi et al., 2008; Mollo et al., 2012a). The higher tendency of the SiO_2-poor, Fe-rich liquids for a slight preferential crystallization of spinel on Pt substrata, as observed in our run-products (Table 2), possibly relies on an enrichment of iron and its fast diffusion in these melts driven by solubility of this element in Pt (especially at low fO_2 conditions) or by

heterogeneous nucleation on the Pt interface without a presence of an iron chemical gradient towards the rim of run-products (Berkebile and Dowty, 1982; Lasaga, 1997; Zhang, 2008). However, whatever the reasons for this experimental observation, the high homogeneity of crystal distribution in the SiO_2-poor, Fe-rich sample charges (Table 2) indicates that only small rim portions near the Pt walls for these run-products (Fig. 2) are affected by preferential crystallization of spinels; in turn, the inner and intermediate portions of these run-products nucleate homogeneously.

Only the $B_{60}R_{40}$ and $B_{40}R_{60}$ run-products from E1 show an inhomogeneous distribution of crystals and both compositions are the lowest reproducible in the E1-E2 experiments (Table 2). Additionally, the two B_{100} run-products from E4-E5, albeit highly homogeneous, are the least reproducible in clinopyroxene content with a difference of about 10 area% (Table 2 and Figure 4). Hence, the homogeneous distribution of crystalline phases inside sample charges is a necessary, although not sufficient, criterion to assess the reproducibility of crystallization experiments. Now, the question is: why only these particular combinations of melt composition and cooling rate are so sensitive to the crystallization path?

A theoretical background to explain this behaviour is provided by time-temperature-transformation (TTT) diagrams. The TTT curves represent experimental products with a certain degree of crystallization produced by annealing at constant temperature for various times. If data are available for different degrees of crystallization, it is possible to correlate the nucleation rate (I), degree of undercooling (ΔT), and induction time (τ^*), i.e. the time required to initiate nucleation of a crystalline phase (Lasaga, 1997; Fokin et al., 2003). In general, the nucleation rate of silicate melts can span ten to twenty orders of magnitude in a 1300-800 °C thermal range; moreover, the variation of nucleation rate progressively increases when approaching to I_{max} (Lasaga, 1997; Fokin et al., 2003: Hersum and Marsh, 2006; Roskovz et al., 2006). The nucleation rate is close to its maximum value I_{max} when a

cooling rate intersects a TTT curve around its tip (Figure 7; Fokin et al., 2003; Iezzi et al., 2009). A graphical summary of these concepts is displayed in Figure 7 for SiO_2-rich (in red) and SiO_2-poor (in blue) melts. Here, the TTT curves represent the onset of crystallization for a given undercooling and time. The silica-rich melt may be either a pure melt or a residual melt after partial crystallization, provided that heterogeneous nucleation on early-formed crystals is negligible.

Using these schematic TTT curves, three general cases of high (H), intermediate (I) and low (L) cooling rates can be distinguished. At the high cooling rate (H) the TTT curve is not intersected for any of the melts under investigation and the melt solidifies to a glass. Based on our experiments, this is the case for cooling rates >>30°C/min. At the intermediate cooling rate (I) the TTT curves of SiO_2-rich melts are still not touched while for the SiO_2-poor melt (for instance B_{100}) the TTT curve is readily intersected. This is the case for a cooling rate of 30 °C/min and, hence, it can be concluded that this rate is close to the critical cooling rate (CCR) for B_{100}. At slow cooling (L), i.e. 0.0167°C/min, for all melt compositions the TTT curves are intersected due to the presence of crystals (Table 2 and Figures 2), but for the most SiO_2-rich composition only for short time. This rate corresponds to the CCR of a melt such as R_{100}. As a function of the initial melt composition, the TTT curves can be intersected at high temperature (small ΔT), i.e. significantly above the temperature of I_{max}. Under this condition, only few nuclei are formed and the growth rate is fast (Lasaga, 1997). As a consequence the crystallized products are composed of early-formed large crystals. The trend of increasing crystal size with decreasing cooling rate observed here (Fig. 2) is consistent with this scenario.

By contrast, when a cooling rate intersects a TTT curve around its tip (Fig. 7), the nucleation rate is close to I_{max} and even a small variation in the local temperature may have a strong effect on the initial number of forming crystals (nuclei); this can explain the large

variation in abundance of small plagioclase crystals in $B_{60}R_{40}$ and $B_{40}R_{60}$ run-products from E1-E2. In these two duplicated experiments, after the crystallization of spinel and large clinopyroxene as a result of the intersection of a cooling rate L with the TTT blue line above I_{max}, the produced residual melt represented by the TTT red line can be intercepted around its tip to produce plagioclase nuclei (Fig. 7). The number of nuclei will strongly depend on the time for which the system remains within the TTT loop. The same is the case for the time available for the crystal growth. Hence, large variation in crystal number and size can be the result of small variations in cooling rate and melt composition (induced by small thermal gradient) and, as a consequence, the reproducibility can be poor. A similar explanation is plausible for the low reproducibility of E4-E5 run-products; in Figure 7 this is represented by a cooling rate L that intercepts the blue line (B_{100}) at its tip. In agreement, the comparison of clinopyroxene in B_{100} run-products from E4-E5 and plagioclase in $B_{60}R_{40}$ run-products from E1-E2 evidence a low but detectable difference of the crystal number per area% (Figures 2a and 2c), possibly related to the proposed scenario. An even more cogent difference in plagioclase number density and amount is that of $B_{40}R_{60}$ in E1 in comparison with E2 (Table 2); moreover, the $B_{60}R_{40}$ and $B_{40}R_{60}$ run-products from E1 have an inhomogeneous distribution of plagioclase (Table 2), which is indicative for the presence of a thermal gradient when approaching the TTT curve of the residual melt (TTT red line in Figure 7). It is also possible that some textural inhomogeneities are present in one of the two B_{100} run-products from E4-E5, but the very small size of these crystals prevents a direct inspection (Fig. 2c). To summarise, the difference of clinopyroxene plus spinel crystallization in B_{100} (from E4-E5) reflects a situation depicted by an intermediate cooling rate that intercepts the tip of a TTT curve of a SiO_2-poor melt (Fig. 7), whereas the textural difference of lately crystallized plagioclase microlites in $B_{60}R_{40}$ and $B_{40}R_{60}$ samples (from E1-E2) is schematically represented by a low cooling rate (black straight line named L in Figure 7).

5. CONCLUSIONS

The outcomes attained in this study and the open questions raised up from these results can be summarized as follows:

1. a weak preferential nucleation at only few microns from the Pt substrate has been observed for all the run-products with composition between B_{100} and $B_{60}R_{40}$, whereas between $B_{40}R_{60}$ and R_{100} compositions the nucleation results are unaffected by Pt walls;

2. all the six bulk compositions cooled at identical rate, but run with a huge difference in superheating path (S1-E3), are always reproducible as demonstrated by phase proportions;

3. depending on the bulk composition, some cooling conditions are more sensitive than others to give less reproducible results;

4. due to the importance of the bubble size and the composition of trapped gas in determining crystal nucleation, future experiments are necessary to better asses these aspects;

5. experimental TTT diagrams are of paramount importance to quantify the nucleation rate and related induction time of chemically complex silicate melts;

6. results from solidification experiments can be appropriately interpreted and compared among them only if dissolved H_2O contents, bubbles and unmelted solid phase amounts, as well as iron speciation are determined before inducing crystallization processes;

7. from basaltic to rhyolite melts the intrinsic ability to produce a glass (glass-forming ability) is larger than 3 order of magnitudes (> 30 and < 0.0167 °C/min, respectively) (Fig. 3).

The experimental conditions used here are not directly relevant for many natural processes since nearly anhydrous and extremely oxidised starting liquids are involved. However, due to the similar effects of high temperature and long time in eliminating the

preferential nucleation sites above liquidus conditions, rationally we can infer that natural silicate liquids superheated few °C above their liquidus from months to years would minimize the number of heterogeneous sites showing a re-homogenisation process similar to that observed in our silicate liquids (Fig. 6). Similar silicate liquids in natural environments can be aphyric lavas and dikes at shallower crustal levels, for instance in mid-ocean ridges.

Acknowledgements

This study was supported by "Fondi Ateneo of the University G. d"Annunzio" and PRIN project "Experimental determination of the glass-forming ability (GFA), nucleation and crystallization of natural silicate melts" awarded to Gianluca Iezzi. The authors thank Julia Hammer for a critical review of the manuscript, D. Dolfi and G. De Astis for providing the starting materials (i.e. B_{100} and R_{100}, respectively) and G. Torresi for the preparation of the intermediate glassy compositions (i.e. $B_{80}R_{20}$, $B_{60}R_{40}$, $B_{40}R_{60}$, $B_{20}R_{80}$). F. Vetere is supported by a Marie Curie fellowship SolVoM #297880. S. Mollo is supported by ERC Starting Grant GLASS (#259256).

REFEENCES

Armienti, P., 2008. Decryption of igneous rock textures: crystal size distribution tools. In: Putirka, K.D., Tepley, F.J. (Eds.), Minerals, Inclusions and Volcanic Processes: Reviews in Mineralogy and Geochemistry 69, 623-650.

Behrens, H., Romano, C., Nowak, M., Holtz, F., Dingwell, D.B. 1996. Near-infrared spectroscopic determination of water species in glasses of the system MAlSi 3O 8 (M = Li, Na, K) : An interlaboratory study**.** Chemical Geology 128, 41-63.

Berkebile, C.A., Dowty, E., 1982. Nucleation in laboratory charges of basaltic composition. American Mineralogist 67, 886-899.

Chakraborty, S., 1995. Diffusion in silicate melts. In: Stebbins JF, Dingwell DB, McMillan PW (Eds) Structure and Dynamics of silicate melts: Reviews in Mineralogy and Geochemistry 32, 411-497.

Corrigan, G.M., 1982. Supercooling and the crystallization of plagioclase, olivine, and clinopyroxene from basaltic magmas. Mineralogical Magazine 46, 31-42.

Couch, S., 2003. Experimental investigation of crystallization kinetics in a haplogranite system. American Mineralogist 88, 1471-1485.

Davies, M.J., Ihinger, P.D., 1998. Heterogeneous crystal nucleation on bubbles in silicate melts. American Mineralogist 83, 1008-1015.

Del Gaudio, P., Mollo, S., Ventura, G., Iezzi, G., Taddeucci, J., Cavallo, A., 2010. Cooling rate-induced differentiation in anhydrous and hydrous basalts at 500 MPa: Implications for the storage and transport of magmas in dikes. Chemical Geology 270,164–178.

Dingwell, D.B., Webb, S.L., 1990. Relaxation in silicate melts. European Journal of Mineralogy 2, 427-449.

Dingwell, D.B., 1995. Relaxation in silicate melts: some applications in petrology. In: Stebbins JF, Dingwell DB, McMillan PW (Eds.), Structure and Dynamics of Silicate Melts: Reviews in Mineralogy and Geochemistry 32, 21-66.

Dingwell, D.B., 2006. Transport properties of magmas: diffusion and rheology. Elements 2, 281-286.

Donaldson, C.H., Williams, R.J., Lofgren, G., 1975. Sample holding technique for study of crystal growth in silicate melts. American Mineralogist 60, 324-326.

Dowty, E., 1980. Crystal growth and nucleation theory and the numerical simulation of igneous crystallization. In: Hargraves RB (Ed.), The Physics of Magmatic Processes, Princeton University Press, pp 419-485.

Fenn, P.M., 1977. The nucleation and growth of alkali feldspars from hydrous melts. Canadian Mineralogist 15, 135-161.

Fokin, V.M., Zanotto, E.D., Schmelzer, J.W.P., 2003. Homogeneous nucleation versus glass transition temperature of silicate glasses. Journal of Non-Crystalline Solids321, 52-65.

Gibb, F.G.F., 1974. Supercooling and crystallization of plagioclase from a basaltic magma. Mineralogical Magazine 39, 641-653.

Hammer, J.E., 2006. Influence of fO_2 and cooling rate on the kinetics and energetics of Fe-rich basalt crystallization. Earth and Planetary Science Letters 248, 618-637.

Hammer, J.E., 2008. Experimental studies of the kinetics and energetics of magma crystallization. In: Putirka KD, Tepley FJ (Eds.): Reviews in Mineralogy and Geochemistry 69, 9-59.

Iezzi, G., Mollo, S., Ventura, G., Cavallo, A., Romano, C., 2008. Experimental solidification of anhydrous latitic and trachytic melts at different cooling rates: the role of nucleation kinetics. Chemical Geology 253, 91-101.

Iezzi, G., Mollo, S., Ventura, G., 2009. Solidification behaviour of natural silicate melts and volcanological implications. In: Lewis N, Moretti A (Eds.): Volcanoes: formation, eruptions and modelling, Nova publishers, New York, 127-151.

Iezzi, G., Mollo, S., Torresi, G., Ventura, G., Cavallo, A., Scarlato, P., 2011. Experimental solidification of an andesitic melt by cooling. Chemical Geology 283, 261-27.

Klöß, G.H., 2000. Dichtefluktuationen natürlicher Gläser. Dissertation, Universtiy of Jena

Lasaga, A.C., 1997. Kinetic Theory in the Earth Sciences. Princeton University Press, Princeton, NY.

Le Maitre, R.W., Streckeisen, A., Zanettin, B., Le Bas, M.J., Bonin, B., Bateman, P., Bellieni, G., Dudek, A., Efremova, S., Keller, J., Lamere, J., Sabine, P.A., Schmid, R., Sorensen, H,, Woolley, A.R., 2002. Igneous Rocks: A Classification and Glossary of Terms, Recommendations of the International Union of Geological Sciences, Subcommission of the Systematics of Igneous Rocks. Cambridge University Press, Cambridge.

Lofgren, G., 1980. Experimental studies on the dynamic crystallisation of silicate melts. In: Hargraves, R.B. (Ed.), Princeton University Press, Princeton, NY.

Lofgren, G., 1983. Effect of heterogeneous nucleation on basaltic textures: a dynamic crystallization study. Journal of Petrology 24, 229-255.

Kirkpatrick, R.J., 1981. Kinetics of crystallization of igneous rocks. In: Lasaga, A.C., Kirckpatrick, R.J. (Eds.): Reviews in Mineralogy and Geochemistry 8, 321-397.

Martel, C., Schmidt, B., 2003. Decompression experiments as an insight into ascent rates of silicic magmas. Contributions to Mineralogy and Petrology 144, 397-415.

Misiti, V., Vetere, F., Mangiacapra, A., Behrens, H., Cavallo, A., Scarlato, P., Dingwell, D.B., 2009. Viscosity of high-K basalt from the 5th April 2003 Stromboli paroxysmal explosion. Chemical Geology 260, 278-285.

Mollo, S., Putirka, K., Iezzi, G., Del Gaudio, P., Scarlato, P., 2011. Plagioclase-melt (dis)equilibrium due to cooling dynamics: implications for thermometry, barometry and hygrometry. Lithos 125, 221-235.

Mollo, S., Iezzi, G., Ventura, G., Cavallo, A., Scarlato, P., 2012a. Heterogeneous nucleation mechanisms and formation of metastable phase assemblages induced by different crystalline seeds in a rapidly cooled andesitic melt. Journal of Non-Crystalline Solids358, 1624-1628.

Mollo, S., Putirka, K., Iezzi, G., Scarlato, P., 2012b. The control of cooling rate on titanomagnetite composition: Implications for a geospeedometry model applicable to alkaline rocks from Mt. Etna volcano. Contributions to Mineralogy and Petrology, doi: 10.1007/s00410-012-0817-6.

Moynihan, C.T., 1995. Structural relaxation and the glass transition. In: Stebbins, J.F., Dingwell, D.B., McMillan, P.W. (Eds.) Structure and Dynamics of Silicate Melts: Reviews in Mineralogy and Geochemistry 32, 1-20.

Muller, R., Zanotto, E.D., Fokin, V.M., 2000. Surface crystallization of silicate glasses: nucleation sites and kinetics. Journal of Non-Crystalline Solids274, 208-231.

Pupier, E., Duchene, S., Toplis, M.J., 2008. Experimental quantification of plagioclase crystal size distribution during cooling of a basaltic liquid. Contribution to Mineralogy and Petrology. Doi:10.1007/s00410-007-0258-9.

Richet, P., 2002. Enthalpy, volume and structural relaxation in glass-forming silicate melts. J Therm Anal Calorim 69, 739-750.

Roskosz, M., Toplis, M.J., Besson, P., Richet, P., 2005. Nucleation mechanisms: a crystal chemical investigation of phases forming in highly supercooled aluminosilicate liquids. Journal of Non-Crystalline Solids351, 1266-1282.

Schiavi, F., Walte, N., Konschak, A., Keppler, H., 2010. A moissanite cell apparatus for optical in situ observatyion of crystallising melts at high temperature. American Mineralogist 95, 1069-1079.

Schuessler, J.A., Botcharnikov, R.E., Behrens, H., Misiti, V., Freda, C., 2008. Oxidation state of iron in hydrous phono-tephritic melts. American Mineralogist 93, 1493-1504,

Stebbins, J.F., 1995. Dynamics and structure of silicate and oxide melts: nuclear magnetic resonance studies. In: Stebbins, J.F., Dingwell, D.B., McMillan, P.W. (Eds.)

Structure and Dynamics of Silicate Melts: Reviews in Mineralogy and Geochemistry 32, 191-246.

Swanson, S.E., 1977. Relation of nucleation and crystal-growth rate to the development of granitic textures. American Mineralogist 62, 966-978.

Sycheva, G.A., 2009. Influence of the presence of bubbles on the parameters of crystal nucleation in the $26Li_2O \cdot 74SiO_2$ glass. Glass Physics and Chemistry 35, 602-612.

Tsuchiyama, A., 1983. Crystallization kinetics in the system $CaMgSi_2O_6$-$CaAl_2Si_2O_8$: the delay in nucleation of diopside and anorthite. American Mineralogist 68, 687-698.

Vetere, F., Behrens, H., Schuessler, J.A., Holtz, F., Misiti, V., Borchers, L., 2008. Viscosity of andesite melts and its implication for magma mixing prior to Unzen 1991 – 1995 eruption. Journal of Volcanology and Geothermal Research 175, 208-217.

Webb, S.L., 1997. Silicate melts: relaxation, rheology, and the glass transition. Reviews in Geophysics 35, 191-218.

Webb, S.L., 2005. Silicate melts at extreme conditions. In: Miletich, R., (Ed.): Mineral behaviour at extreme conditions, EMU Notes in Mineralogy 7, 65-94.

Wilson, A.D., 1960. The micro-determination of ferrous iron in silicate minerals by a volumetric and colorimetric method. Analyst 85, 823-827.

Zhang, Y., Xu, Z., Liu, Y., 2003. Viscosity of hydrous rhyolitic melts inferred from kinetic experiments, and a new viscosity model**.** American Mineralogist 88, 1741-1752.

Zhang, Y., 2008. Geochemical kinetic. Princeton University Press, Princeton, NY.

TABLES

Table 1. Chemical compositions of the six glass starting materials.

Footnotes: major components are in weight %, H_2O is in ppm, and density in g/cm^3. TAS refers to the classification scheme of Le Maitre et al. (2002); standard deviation are reported in parentheses.

Table 2. Experimental conditions and textural features of run-products.

Footnotes. Area and sd data are in %; *: presence of small amounts (<1 area%) of extraneous phases such as orthopyroxene, olivine and melilite; sd: standard deviation computed on at least four representative BS-SEM images; H and IN indicate the homogeneous and inhomogeneous distributions of crystals inside a run-product, respectively; LP and A indicate a low preferential nucleation (mainly for sp) and the absence of preferential nucleation on Pt-capsules, respectively; cpx, sp, plg and min refer to: clinopyroxene, spinel and plagioclase and minutes, respectively.

FIGURE CAPTIONS

Fig. 1. Schematic thermal paths used in this study; it has been especially drawn to highlight the different heat treatment of the experiment S1(red path) compared with E1, E2, E3, E4 and E5 (blue path) before cooling. The liquidus temperatures of B_{100} and R_{100} end-member melt compositions are also reported.

Fig. 2. Comparisons of textural features by means of back-scattered FE-SEM images; duplicated run-products, i.e. same starting composition and cooled with the same cooling rate, are compared at the same magnifications. R_{100} run-products are not shown because are almost glassy, i.e. crystal content <1 area%. a) The E1-E2 duplicated run-products solidified from B_{100}, $B_{80}R_{20}$ and $B_{20}R_{80}$ starting compositions show similar textural features, whereas $B_{60}R_{40}$ and $B_{40}R_{60}$ exhibit similar textures for spinel and clinopyroxene but different for plagioclase. b) The S1-E3 run-products show similar textural features, albeit their different heat treatments before the cooling rate of 3 °C/min. c) The two duplicated B_{100} run-products from E4-E5 show similar textural features.

Fig. 3. Comparison of the crystal content (area%) for the experiments E1-E2 (left), S1-E3 (central) and E4-E5 (right). In the limit of their standard deviations, only B_{100} from E4-E5, $B_{60}R_{40}$ from E1-E2 and $B_{40}R_{60}$ from E1-E2 differ in the crystal content (see also Table 2).

Fig. 4. Comparisons of clinopyroxene plus spinel content (area%) for duplicated run-products from E1-E2 (left), S1-E3 (central) and E4-E5 (right) experiments. In the limit of their standard deviations, only the duplicated B_{100} run-products from E4-E5 have different crystal contents (see also Table 2).

Fig. 5. Relaxation times computed via the Maxwell relation (see text) for B_{100} (blue line) and R_{100} (red line) end-member melts as a function of temperature; the liquidus temperatures of these two melts are also indicated.

Fig. 6. Diagram of the minimum diffusion length vs time for different temperatures, constructed by the use of the Eyring relationship (see text). The blue and red lines correspond with B_{100} and R_{100} melts, respectively.

Fig.7. Schematic temperature–time-transformation (TTT) diagrams for hypothetical silicate melts. The red curve represents a silica-rich melt and the blue curve a silica-poor melt. T_{Liq}: liquidus temperature, I_{max}: maximum nucleation rate, H: high cooling rate, I: intermediate cooling rate and L: low cooling rate.

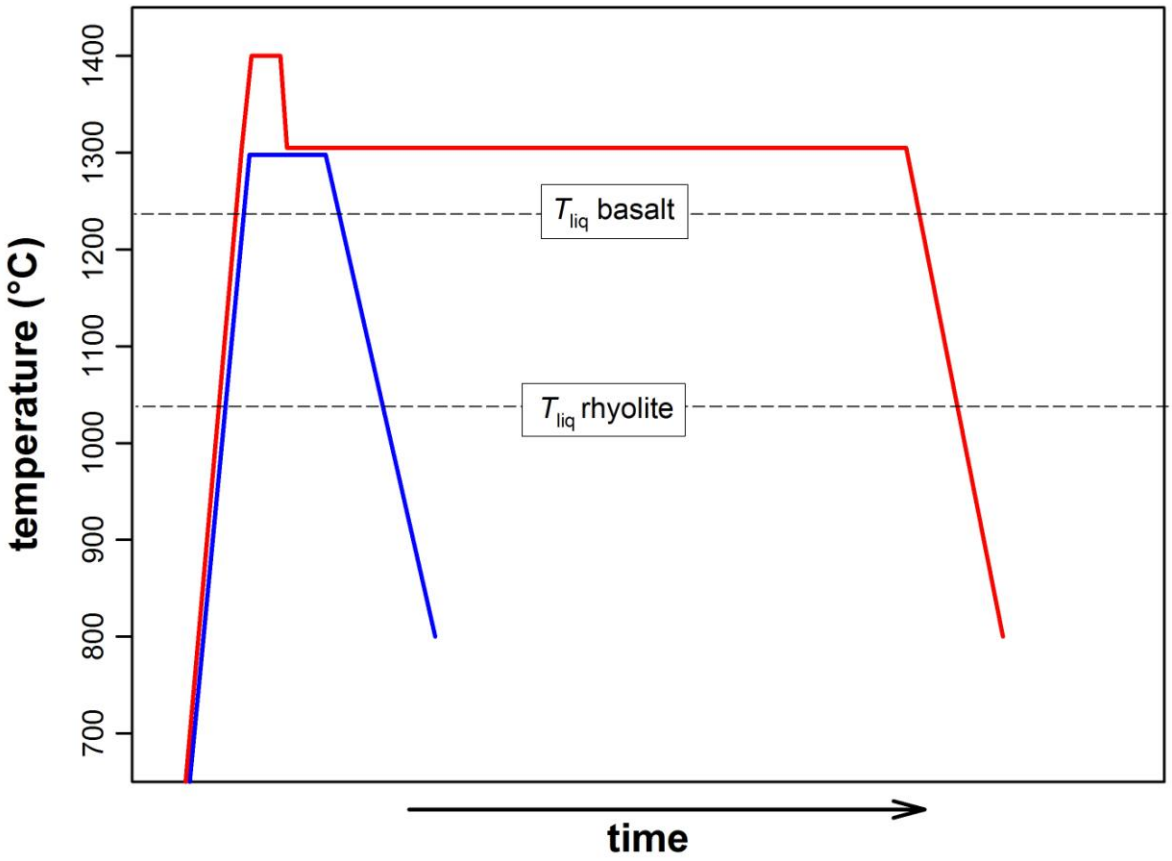

Figure 1

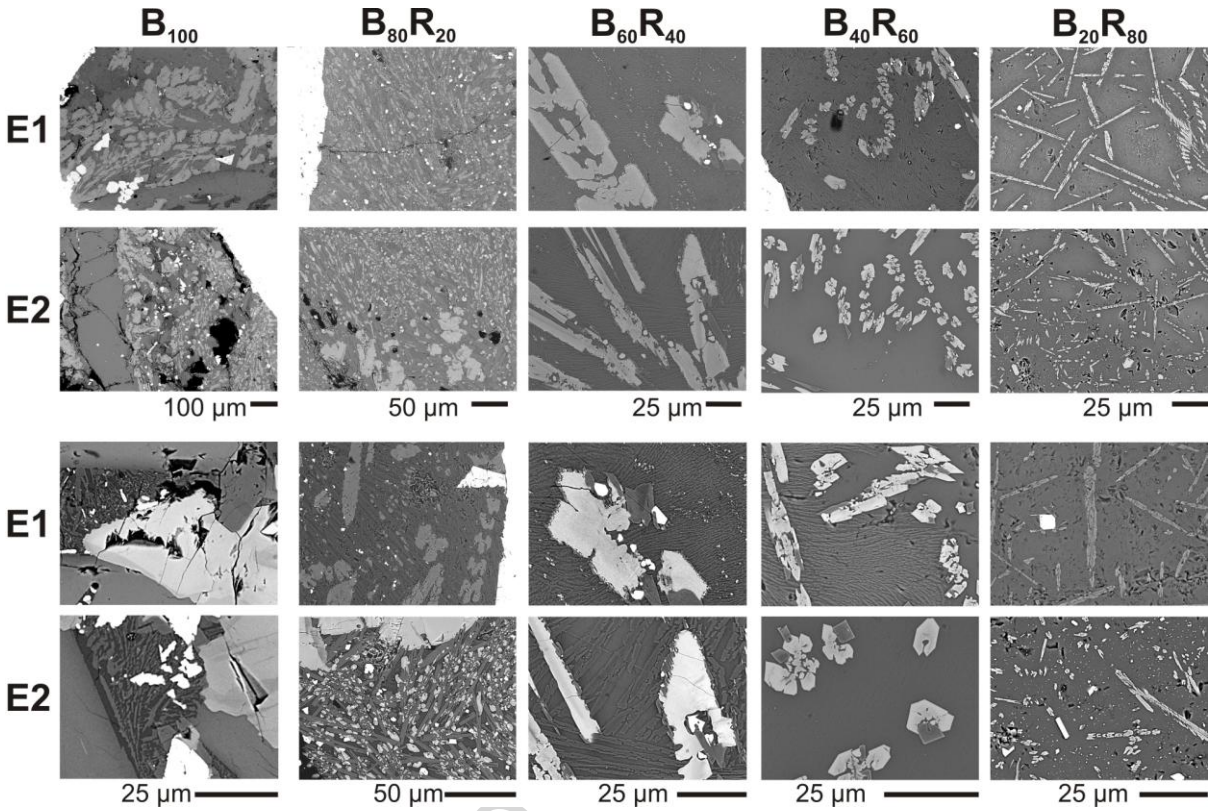

Figure 2a

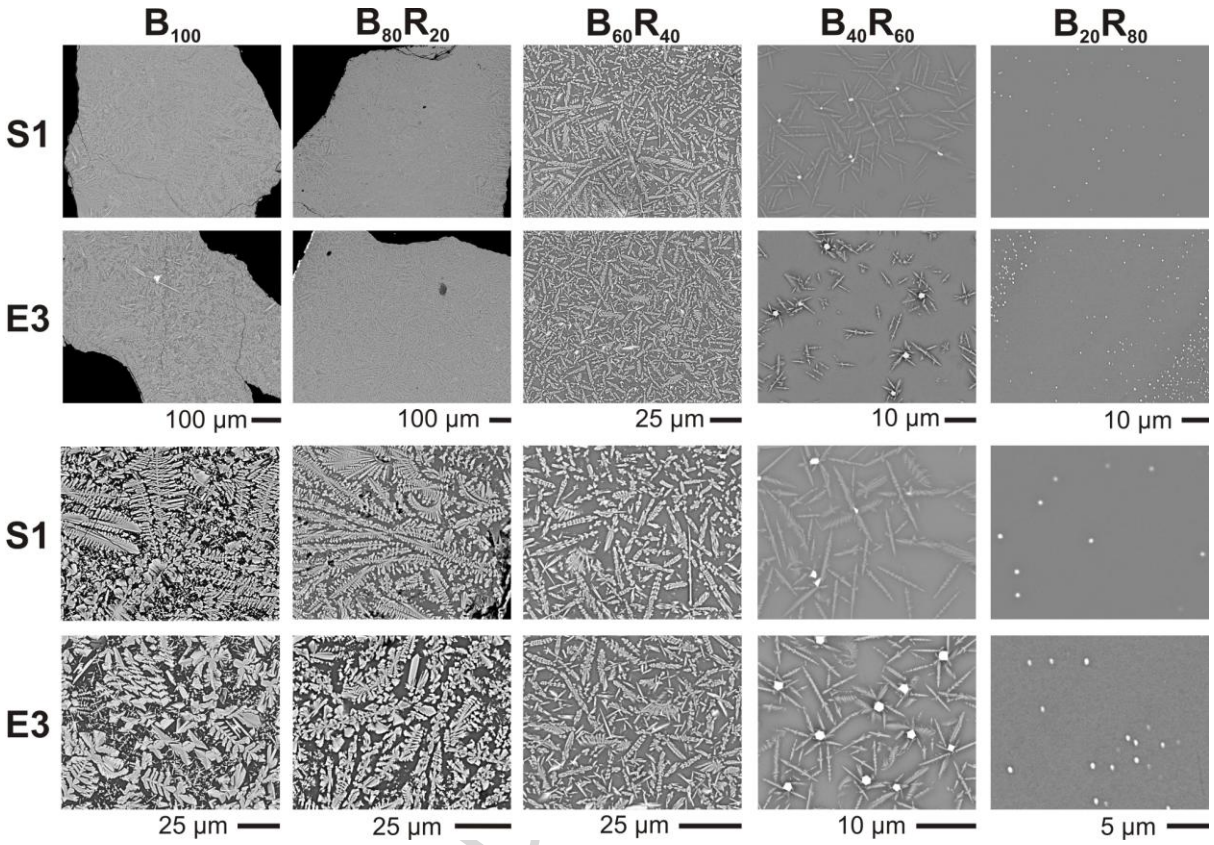

Figure 2b

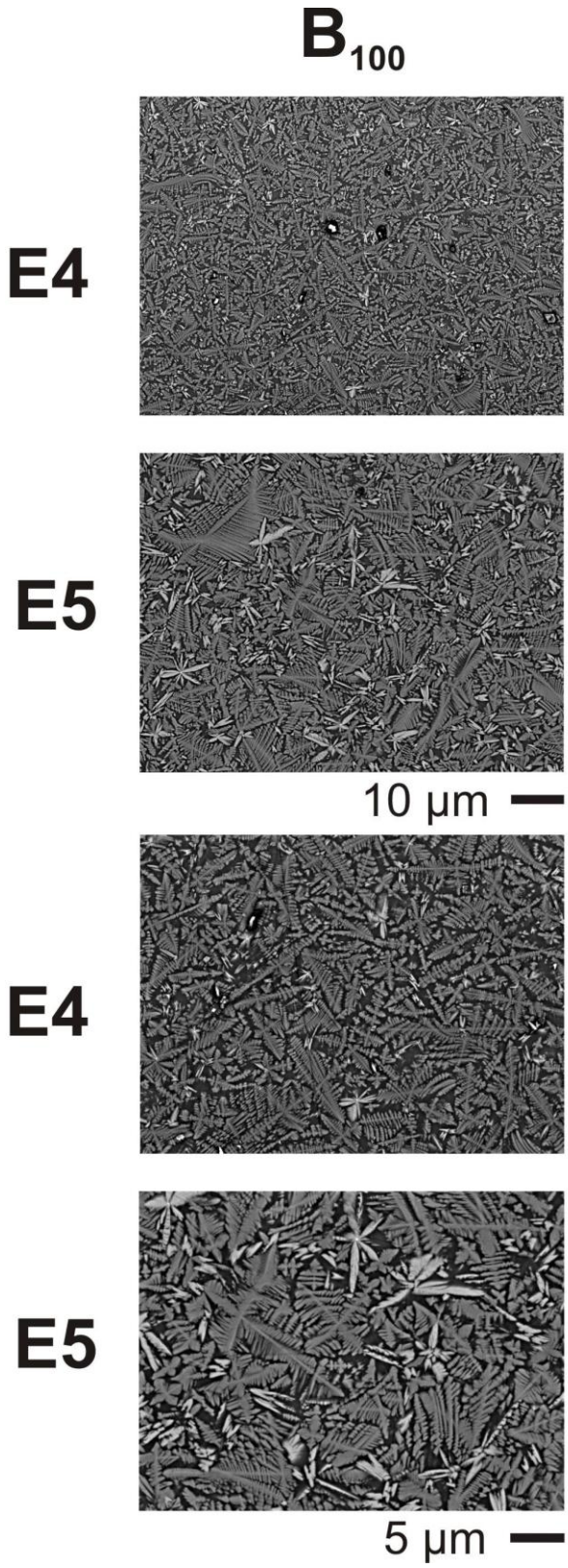

Figure 2c

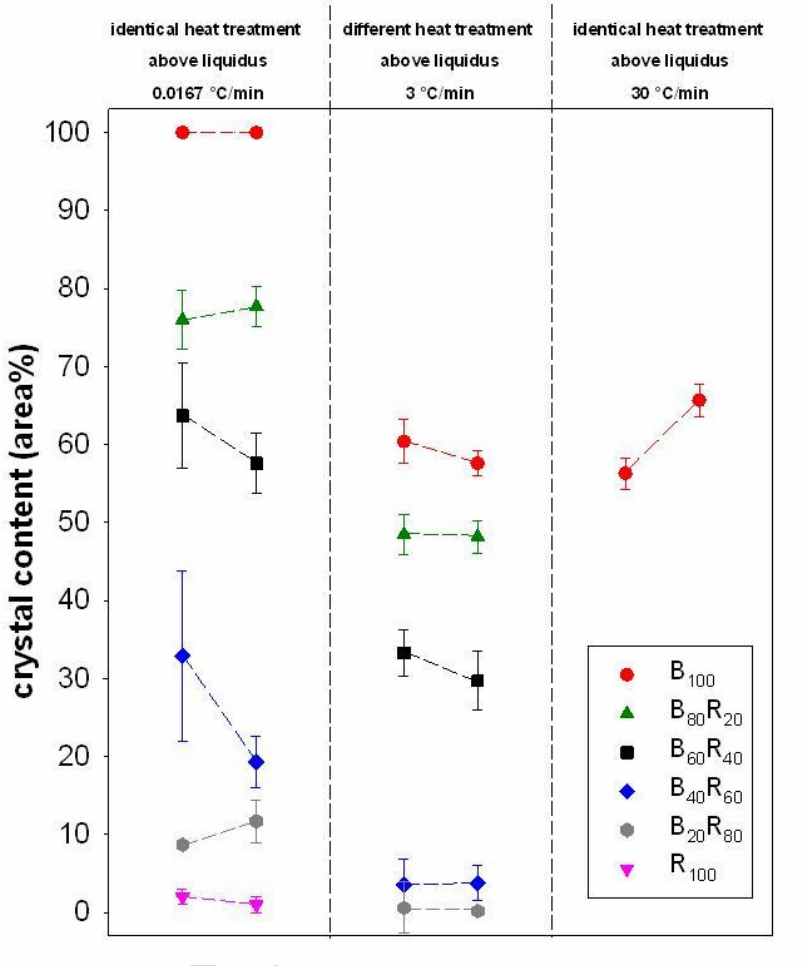

Figure 3

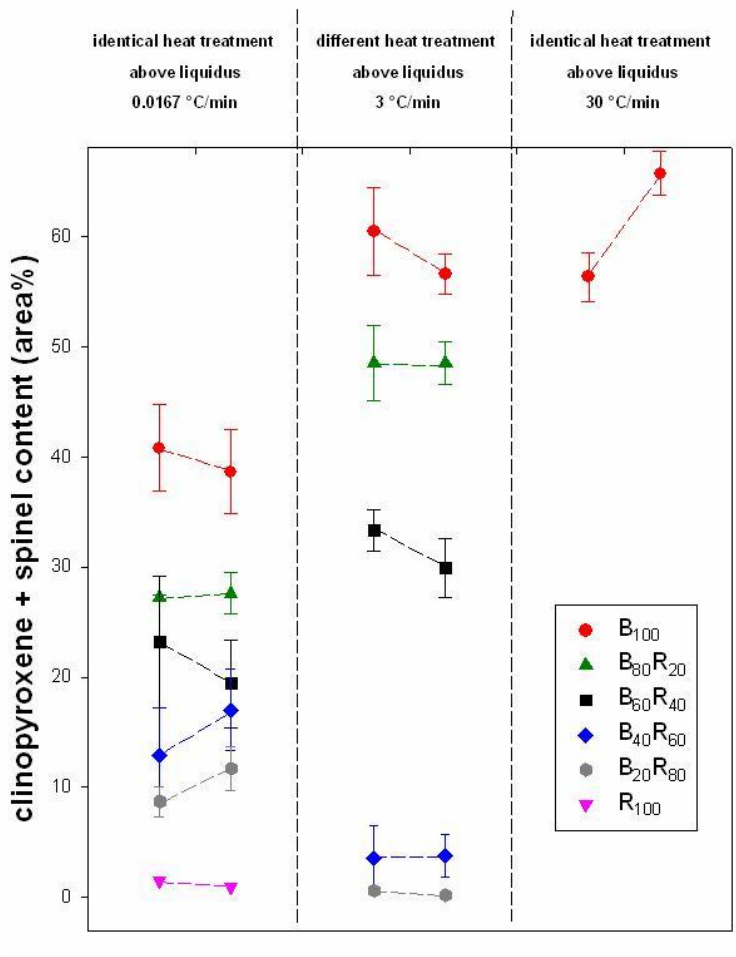

Figure 4

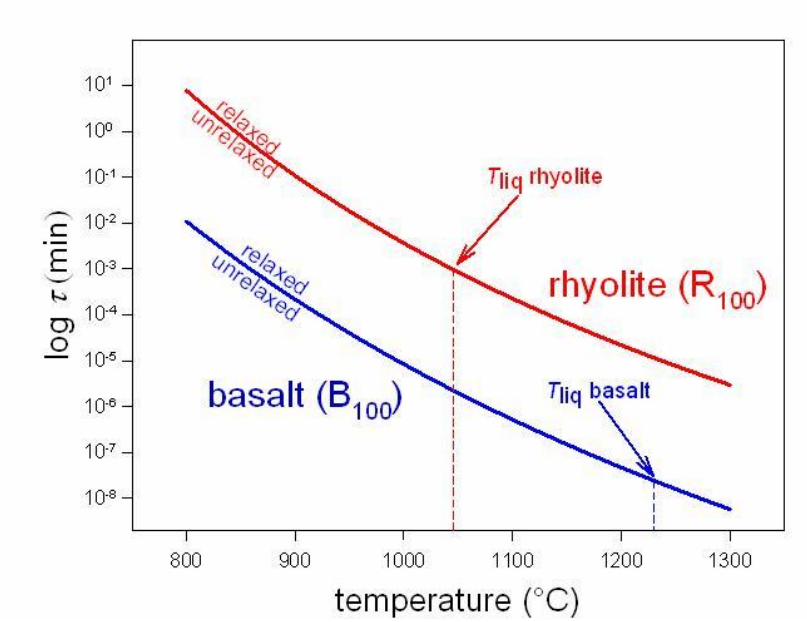

Figure 5

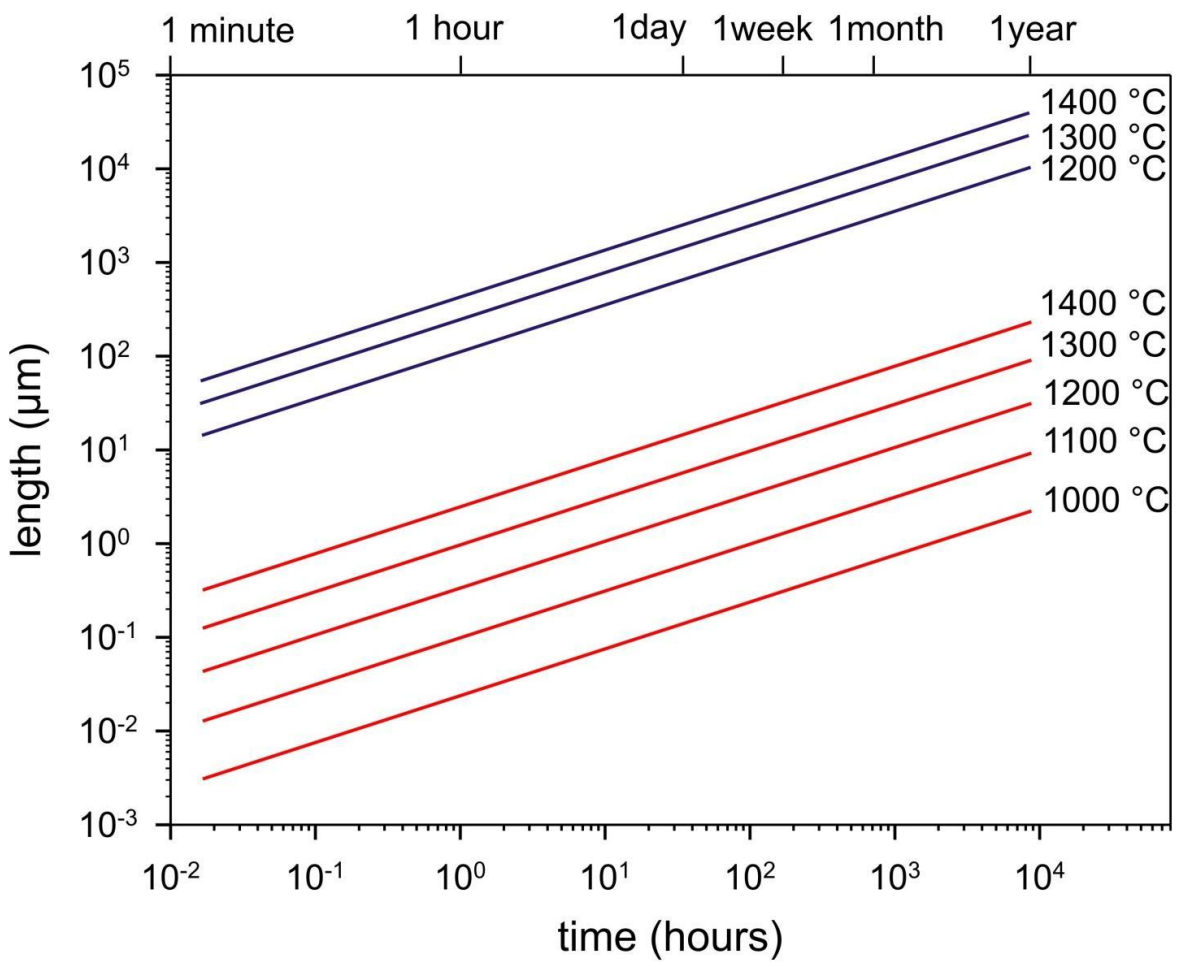

Figure 6

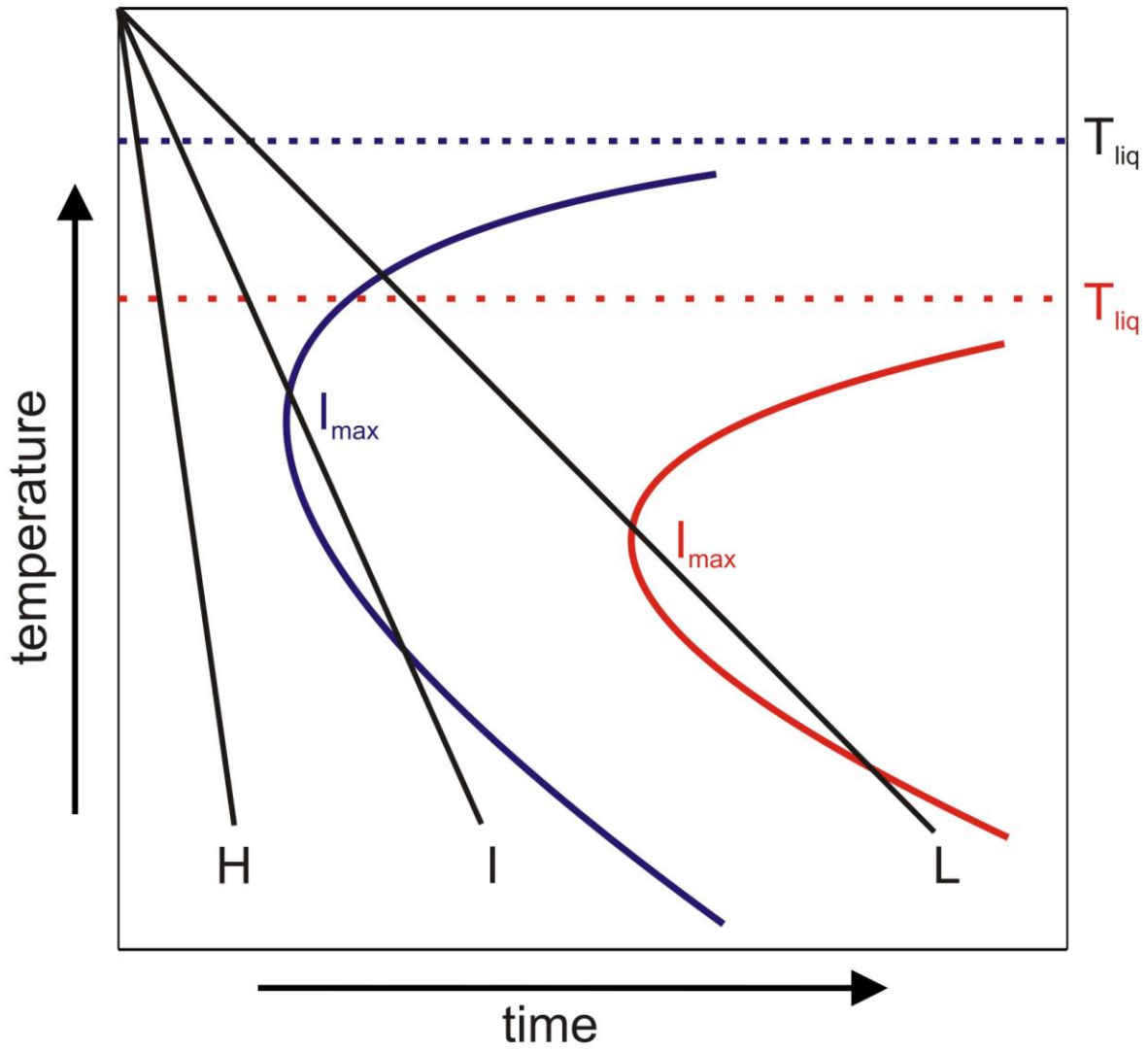

Figure 7

TABLES

Table 1. Chemical compositions of the six glass starting materials.

label	SiO_2	TiO_2	Al_2O_3	Fe_2O_3	MnO	MgO	CaO	Na_2O	K_2O	P_2O_5	total	H_2O	Fe^{2+}/Fe_{tot}	density	TAS
B_{100}	48.02 (0.40)	0.98 (0.08)	15.59 (0.19)	11.37 (0.25)	0.18 (0.04)	9.42 (0.11)	13.20 (0.14)	1.79 (0.05)	0.04 (0.01)	0.06 (0.02)	100.65 (0.67)	53 (13)	0.387 - 0.385 (0.02)	2.757	basalt
$B_{80}R_{20}$	53.01 (0.30)	0.80 (0.06)	14.99 (0.12)	9.49 (0.17)	0.15 (0.04)	7.58 (0.10)	10.79 (0.16)	2.18 (0.07)	1.02 (0.03)	0.02 (0.02)	100.04 (0.36)	157 (7)	0.458-0.440 (0.02)	2.672	basaltic andesite
$B_{60}R_{40}$	57.97 (0.44)	0.65 (0.06)	14.62 (0.27)	7.73 (0.16)	0.13 (0.03)	5.81 (0.08)	8.46 (0.13)	2.59 (0.07)	1.99 (0.05)	0.04 (0.02)	99.99 (0.46)	204 (8)	0.438-0.430 (0.02)	2.600	andesite
$B_{40}R_{60}$	62.73 (0.54)	0.46 (0.05)	14.05 (0.17)	6.02 (0.15)	0.12 (0.04)	4.01 (0.05)	6.07 (0.14)	2.95 (0.07)	3.02 (0.04)	0.02 (0.02)	99.45 (0.73)	238 (4)	0.416-0.412 (0.02)	2.525	andesite
$B_{20}R_{80}$	67.91 (0.38)	0.29 (0.05)	13.59 (0.21)	4.10 (0.20)	0.11 (0.03)	2.18 (0.09)	3.63 (0.13)	3.29 (0.07)	3.99 (0.06)	0.02 (0.02)	99.10 (0.36)	384 (20)	0.437-0.412 (0.04)	2.454	dacite
R_{100}	73.97 (0.67)	0.12 (0.06)	13.48 (0.17)	2.29 (0.16)	0.08 (0.05)	0.44 (0.05)	1.36 (0.08)	3.75 (0.17)	4.89 (0.08)	0.03 (0.02)	100.41 (0.84)	250 (85)	0.340-0.344 (0.02)	2.368	rhyolite

Footnotes: major components are in weight %, H_2O is in ppm, and density in g/cm^3. TAS refers to the classification scheme of Le Maitre et al. (2002); standard deviation are reported in parentheses

Table 2. Experimental conditions and textural features of run-products.

		duplicated run-products				different heat treatment				duplicated run-products			
experimental labels		E1		E2		S1		E3		E4		E5	
heating rate (°C/min)		7		7		7		7		7		7	
dwell temperature (°C)		1300		1300		§1400 - 1300		1300		1300		1300	
Dwell time (min)		120		120		§30 - 2400		120		120		120	
cooling rate (°C/min)		0,0167		0,0167		3		3		30		30	
quenching temperature (°C)		800		800		800		800		800		800	
	textural features	H, LP		H, LP		H, LP		H, LP		H, LP		H, LP	
	phases	area	sd	area	sd	area	sd	area	sd	area	sd	area	sd
B_{100}	cpx	36.3	3.9	36.2	3.8	56.4	5.0	51.2	1.4	53.3	2.2	61.0	2.0
	sp	4.5	1.8	2.4	1.4	4.0	2.3*	5.4	1.2*	3.0	0.7	4.7	1.2
	plg	59.2	4.0	61.4	3.9	0.0	0.0	0.0	0.0	0.0	0.0	0.0	0.0
	glass	0.0	0.0	0.0	0.0	39.6	2.8	43.3	1.6	43.7	2.3	34.3	2.0
	crystals	100.0	0.0	100.0	0.0	60.4	2.8	56.7	1.6	56.3	2.6	65.7	2.1
	textural features	H, P		H, P		H, P		H, P					
	phases	area	sd	area	sd	area	sd	area	sd				
$B_{80}R_{20}$	cpx	26.2	0.2	24.3	1.9	47.3	3.4	45.9	1.9				
	sp	1.0	0.6	3.3	1.0	1.2	0.8	2.6	1.4				
	plg	48.8	3.9	50.2	4.0	0.0	0.0	0.0	0.0				
	glass	24.0	3.8	22.3	2.5	51.5	2.6	51.6	1.3				
	crystals	76.0	3.8	77.7	2.5	48.5	2.6	48.2	2.1				
	textural features	H, P		H, P		H, A		H, P					
	phases	area	sd	area	sd	area	sd	area	sd				
$B_{60}R_{40}$	cpx	21.5	6.0	17.3	4.0	30.3	1.9	28.5	2.7				
	sp	1.8	1.0	2.1	0.7	3.0	1.0	1.4	1.2				
	plg	40.4	7.2	38.2	4.2	0.0	0.0	0.0	0.0				
	glass	36.3	6.6	42.4	3.8	67.7	2.8	70.3	4.0				
	crystals	63.7	6.7	57.6	3.9	33.3	3.0	29.7	3.8				
	textural features	IN, A		H, A		H, A		H, A					
	phases	area	sd	area	sd	area	sd	area	sd				
$B_{40}R_{60}$	cpx	11.4	4.3	15.7	3.7	3.3	2.9	3.4	1.9				
	sp	1.5	0.9	1.3	0.4	0.3	0.3	0.4	0.3				
	plg	20	12.6	2.3	1.2	0.0	0.0	0.0	0.0				
	glass	67.1	10.9	80.7	3.3	96.4	3.3	96.2	2.3				
	crystals	32.9	10.9	19.3	3.3	3.6	3.3	3.8	2.2				
	textural features	IN, P		H, A		H, A		H, A					
	phases	area	sd	area	sd	area	sd	area	sd				
$B_{20}R_{80}$	cpx	8.4	1.4	10.0	2.0	0.0	0.0	0.0	0.0				
	sp	0.3	0.1	1.7	1.5	0.6	0.2	0.2	0.1				
	plg	0.0	0.0	0.0	0.0	0.0	0.0	0.0	0.0				
	glass	91.3	1.4	88.3	2.7	99.4	0.3	99.8	0.2				
	crystals	8.7	0.4	11.7	2.7	0.6	0.3	0.2	0.1				
R_{100}	textural features	H, A		H, A		H, A		H, A					
	phases	area	sd	area	sd	area	sd	area	sd				

cpx	0.0	0.0	0.0	0.0	0.0	0.0	0.0	0.0
sp	1.5	0.2	1.0	0.2	0.0	0.0	0.0	0.0
plg	0.0	0.0	0.0	0.0	0.0	0.0	0.0	0.0
glass	98.5	0.5	99.0	0.6	100.0	0.0	100.0	100.0
crystals	1.5	0.2	1.0	0.2	0.0	0.0	0.0	0.0

Footnotes. Area and sd data are in %; *: presence of small amounts (<1 area%) of extraneous phases such as orthopyroxene, olivine and melilite; sd: standard deviation computed on at least four representative BS-SEM images; H and IN indicate the homogeneous and inhomogeneous distributions of crystals inside a run-product, respectively; LP and A indicate a low preferential nucleation (mainly for sp) and the absence of preferential nucleation on Pt-capsules, respectively; cpx, sp, plg and min refer to: clinopyroxene, spinel and plagioclase and minutes, respectively.

Highlights

- constraints for the interpretation of dynamic solidification experiments
- interpretation of the superheating effect on successive nucleation features
- reproducibility of textures in dynamic cooling experiments
- intrinsic nucleation and solidification properties of natural silicate melts